THE GEOLOGICAL SOCIETY OF AMERICA®

Variable thermal loading and flexural uplift along the Transantarctic Mountains, Antarctica

Gregory R. Brenn[1], Samantha E. Hansen[1], and Yongcheol Park[2]
[1]Department of Geological Sciences, University of Alabama, Tuscaloosa, Alabama 35487, USA
[2]Korea Polar Research Institute, 26 Songdomirae-ro, Yeonsu, Incheon, 406-840, South Korea

ABSTRACT

The high elevations of the Transantarctic Mountains (TAMs) have been suggested to be flexural in origin, but to date, the thermal contribution to uplift has yet to be quantified. Here, we present new P- and S-wave tomography images of the upper-mantle seismic structure beneath the central to northern TAMs, which reveal two, focused low-velocity anomalies beneath Ross Island and Terra Nova Bay that laterally extend beneath the TAMs front and that are connected by a low-velocity region constrained offshore within the Victoria Land Basin. The focused low velocities are interpreted as shallow regions of partial melt, connected by a broad region of slow (warm) upper mantle associated with Cenozoic extension along the Terror Rift. Thermal loading constraints based on our tomographic results are used to update flexural uplift models for the TAMs. Our findings confirm that thermal buoyancy is a principal component leading to the uplift of the TAMs but suggest that the thermal loading is variable along the TAMs front.

INTRODUCTION

Stretching ~3500 km across Antarctica, with elevations up to ~4500 m, the Transantarctic Mountains (TAMs) represent one of the major Cenozoic mountain ranges in the world. The main phase of uplift occurred ca. 55 Ma (e.g., Fitzgerald, 2002), and today the TAMs separate the stable East Antarctic craton from the West Antarctic Rift System (WARS; Fig. 1). However, the origin of the TAMs is enigmatic because they show no evidence, such as folding and reverse faulting, for a typical Cordilleran-type or continental collision–type orogenesis (e.g., Fitzgerald, 2002). Given this, the TAMs serve as an ideal laboratory in which to investigate the geodynamic processes associated with noncompressional mountain building.

Various mechanisms have been proposed to explain the origin of the TAMs. Some studies (e.g., Studinger et al., 2004) have attributed the TAMs to rift flank uplift and climate-induced erosional unloading, and these models require a thick (~5 km) crustal root to provide isostatic support beneath the mountain range. However, recent studies (Hansen et al., 2009, 2016; Ramirez et al., 2016) have revealed minimal evidence for such a root and instead show that the crustal thickness beneath the TAMs is comparable to that found beneath East Antarctica. Other studies have instead associated the TAMs with a flexural origin (e.g., Stern and ten Brink, 1989; ten Brink et al., 1997), where lateral heat conduction from hotter mantle beneath the WARS provides a thermal load along the edge of the East Antarctic lithosphere, leading to broad-scale flexure and uplift. Previously generated continental-scale (e.g., Morelli and Danesi, 2004; Hansen et al., 2014) and regional-scale (Watson et al., 2006; Lawrence et al., 2006) seismic tomography images revealed slow upper-mantle velocities beneath Ross Island (RI; Fig. 1), which extend vertically to ~300 km depth and laterally ~50–100 km inland beneath the central TAMs front. This structure is likely consistent with the thermal load suggested by the flexural origin models; however, the uplift contribution of this thermal load has not been quantified. Further, the spatial resolution of the tomographic images rapidly decreases away from RI because of the lack of seismic station coverage in the northern TAMs; therefore, it is unclear if the anomalous, slow upper-mantle structure continues along strike.

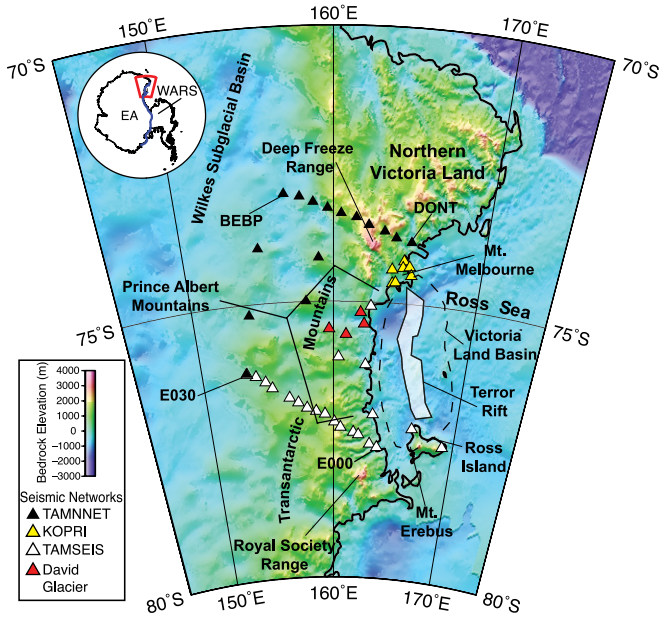

Figure 1. Map of study area in Antarctica. Stations (triangles) are color-coded by network (see the Data Repository [see footnote 1]), and first and last stations along the Transantarctic Mountains Seismic Experiment (TAMSEIS) and the Transantarctic Mountains Northern Network (TAMNNET) transects are labeled. Bedrock topography is from ETOPO1 model (Amante and Eakins, 2009). Dashed black line denotes boundary of Victoria Land Basin, and white shaded region denotes Terror Rift (modified from Bannister et al., 2003). (Inset) Outline of Antarctica. Red polygon highlights study region, and blue line marks boundary between East Antarctica (EA) and West Antarctic Rift System (WARS).

From 2012 to 2015, the Transantarctic Mountains Northern Network (TAMNNET; Fig. 1) was deployed to fill the gap in regional seismic station coverage and to provide data for new, high-resolution imaging of the crustal and upper-mantle structure beneath the northern TAMs (Hansen et al., 2015). Combining data from TAMNNET and from three other regional networks, the current study presents the first regional-scale body wave tomography images of the upper-mantle structure beneath the central and northern TAMs. Our new models are used to assess the along-strike variability of the low upper-mantle velocities between RI and northern Victoria Land (Fig. 1), and thermal loading constraints based on our tomographic results are used to quantify the flexural uplift along the TAMs. We demonstrate that the thermal load varies along strike of the TAMs but serves as a principal component for their uplift and high elevations.

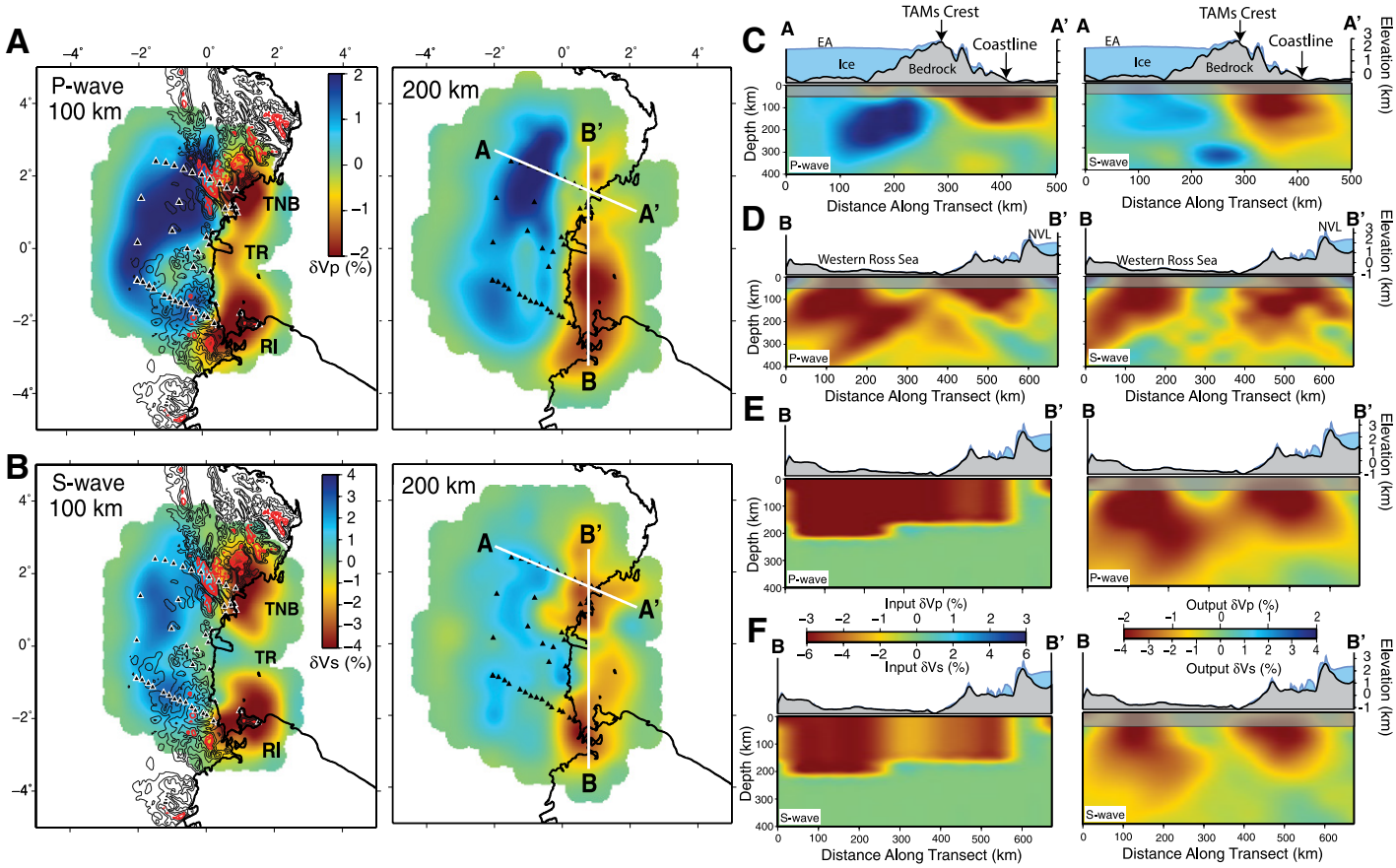

Figure 2. A,B: Map-view slices through our P-wave (A) and S-wave (B) models, highlighting velocity perturbations (δV_P, δV_S). Triangles denote stations (Fig. 1). On 100 km depth panels, black topographic contours represent 500, 1000, and 1500 m, and red contours represent 2000, 2500, and 3000 m from BEDMAP2 (Fretwell et al., 2013). Cross-section locations are shown on 200 km depth panels. TNB—Terra Nova Bay, TR—Terror Rift, RI—Ross Island. (C, D) Vertical cross sections along (C) profile A-A′ and (D) profile B-B′. EA—East Antarctica; TAMs—Trans-antarctic Mountains; NVL—Northern Victoria Land. (E, F) The input and recovered models for the P-wave (E) and S-wave (F) synthetic tests.

RELATIVE TRAVELTIME TOMOGRAPHY

P- and S-wave traveltimes were determined from teleseismic earthquakes recorded by 47 broadband seismic stations deployed throughout Victoria Land and the northern TAMs (Fig. 1). Relative traveltime residuals for these data were calculated with respect to the IASP91 Earth model (Kennett and Engdahl, 1991), corrected for station-specific ice and crustal thicknesses (Hansen et al., 2016). The traveltime residuals were determined using multichannel cross-correlation (VanDecar and Crosson, 1990), implemented with the AIMBAT phase picking tool (Lou et al., 2013), and the data were then inverted using the method of Zhao et al. (1994, and references therein) to create a three-dimensional model of the upper-mantle velocity structure. Goodness of fit was determined by minimizing the root mean square (RMS) misfit before and after the inversion. Our final models reduce the RMS for the P- and S-wave traveltime residuals by ~85% and ~86%, respectively (see the GSA Data Repository[1] for further details).

SEISMIC VELOCITY MODELS

Both our P- and S-wave models (Fig. 2; Fig. DR6 in the Data Repository) reveal fast velocities ($\delta V_P \approx +1.25\%$; $\delta V_S \approx +2.75\%$) beneath East Antarctica, down to ~300 km depth, consistent with a Precambrian craton. Additionally, two prominent slow-velocity anomalies are observed adjacent to the TAMs: one beneath RI ($\delta V_P \approx -2.0\%$; $\delta V_S \approx -2.75\%$) and the other beneath Terra Nova Bay (TNB; $\delta V_P \approx -1.75\%$; $\delta V_S \approx -2.5\%$). The RI anomaly extends vertically to ~250 km depth and laterally ~100 km inland from the Ross Sea coast beneath the TAMs, where it is sharply bounded by the fast East Antarctic velocities (Fig. 2; Fig. DR6). These observations are comparable to those from previous regional studies in the central TAMs (Watson et al., 2006; Lawrence et al., 2006). The TNB anomaly also extends ~100 km laterally inland beneath the northern TAMs, but it is constrained to depths <~150 km (Fig. 2C). In our P-wave model (Figs. 2A and 2D), the RI and TNB anomalies appear to be connected by a region of relatively slow velocity ($\delta V_P \approx -1.5\%$), with a somewhat less pronounced signature than its RI and TNB counterparts. This structure is centered at ~150 km depth (Fig. 2D) and is concentrated offshore along the Ross Sea coast (Fig. 2A)—an area coincident with the Terror Rift (TR), a focused region of rifting and extension in the Victoria Land Basin (Fig. 1). Our S-wave model poorly resolves the slow-velocity connection between the RI and TNB anomalies (Figs. 2B and 2D). Checkerboard (Figs. DR7–DR8) and other synthetic tests (Figs. 2E and 2F; Figs. DR9–DR11) indicate that this is a resolution issue associated with fewer S-wave traveltime residuals, particularly from the David Glacier network (Fig. 1).

DISCUSSION

Until the addition of TAMNNET, upper-mantle velocity variations along strike of the TAMs were largely unconstrained. A recent surface wave model (Graw et al., 2016), which also incorporated the TAMNNET data, highlights slow upper-mantle velocities beneath the TR and the northern TAMs, but this model only constrains structure down to

[1]GSA Data Repository item 2017137, Figures DR1–DR16, are available online at www.geosociety.org/datarepository/2017/ or on request from editing@geosociety.org.

~160 km depth. Further, the body wave tomography approach employed here provides better lateral resolution than the surface wave technique, allowing us to assess the connection between the RI and TNB anomalies in greater detail.

We used synthetic resolution tests along profile B-B′, which runs parallel to the coast, to further assess the slow velocity structure along the TAMs front (Figs. 2E and 2F). Input anomalies with thicknesses of 200 km ($\delta V_P = -3.5\%$, $\delta V_S = -5.5\%$) and 150 km ($\delta V_P = -2.5\%$, $\delta V_S = -4.5\%$) were used to represent the RI and TNB structures, respectively. Additionally, a 150-km-thick anomaly ($\delta V_P = -2.75\%$, $\delta V_S = -3.0\%$) was used to represent the slow RI-TNB connection along the TR. Checkerboard and other resolution tests (Fig. 2; Figs. DR7–DR11) indicate that the recovery of our tomographic models is generally ~60%; therefore, the synthetic anomalies must have higher input amplitudes to recover the observed amplitudes. The recovered models (Figs. 2E and 2F) further highlight the better resolution of our P-wave model compared to our S-wave model, though both models have decreased resolution above ~100 km depth within the TR region. That being said, for both models, the connected geometry best approximates the observed velocity structure along the TAMs (Fig. 2D), and synthetic models without the RI-TNB connection do not match our tomographic images (Figs. DR9–DR11). Together, our tomographic results and synthetic tests provide the first strong evidence that the RI and TNB anomalies are connected and are ultimately part of the same, larger-scale anomalous structure.

Multiple studies have attempted to explain the source of the slow upper-mantle velocities beneath RI. Some investigations attributed the velocity signature to a deep-seated mantle plume (e.g., Kyle et al., 1992; Sieminski et al., 2003), while others instead argued that the low velocities are constrained to depths <~300 km and are associated with rift-related decompression melting at the southern end of the TR (e.g., Rocchi et al., 2005; Reusch et al., 2008; Hansen et al., 2014). Aside from the current study, the TNB anomaly has only been imaged by regional surface wave analyses based on the TAMNNET data (Graw et al., 2016) and by a local P-wave tomographic study based on data from the KOPRI network (Fig. 1; Park et al., 2015). These studies suggested that the TNB anomaly may be associated with either rift-related decompression melting near the northern end of the TR or localized partial melting induced by edge-driven convection beneath the TAMs. Our results indicate that the slow velocities along the TAMs front are constrained to upper-mantle depths; therefore, they are consistent with high-temperature, low-density material associated with lithospheric extension along the TR. Further, the slower signatures of the RI and TNB anomalies may mark "pockets" of decompression melting within the TR. Similar geodynamic structure has been observed, for example, in the Gulf of California, where concentrated slow anomalies within the broader, generally low velocities beneath the rift have been interpreted as regions of focused partial melting, triggered by extension (Wang et al., 2009). Such partial melt would be expected to occur at depths ≤~100 km, but given the overall slow signature of the TR and the resolution of body wave models, the underlying mantle would appear slower beneath RI and TNB. Incipient melting at deeper depths may also occur if small amounts of water or other volatiles are present (Wang et al., 2009).

IMPLICATIONS

The thermal anomaly along the TAMs front, highlighted by the velocity signature in our models, and the uniform crustal structure beneath the mountain range (Hansen et al., 2009, 2016; Ramirez et al., 2016) are most consistent with a flexural origin for the TAMs (e.g., ten Brink et al., 1997, and references therein); however, there is some notable variability. The highest elevations in our study area are located within the Deep Freeze and the Royal Society Ranges (Fig. 1), and these areas sit directly above the TNB and RI anomalies, respectively (Fig. 2). In contrast, the slow upper-mantle velocities between RI and TNB along the TR do not extend laterally beneath the TAMs, which interestingly coincide with the predominantly lower-elevation Prince Albert Mountains (Fig. 1). A strong correlation exists between the variability in the slow upper-mantle structure, and hence the thermal anomalies along the TAMs front, and variability in the topography.

To further assess the flexural origin model, we relate the low-velocity structure from our tomographic images to surface elevation with a velocity-temperature-density relationship and a bending model for a broken elastic plate, similar to Stern and ten Brink (1989) and ten Brink et al. (1997), hereinafter referred to as the 1989 and 1997 models, respectively. These previous studies only crudely estimated the magnitude and distribution of the thermal load beneath the TAMs, but our new high-resolution tomographic models allow us to better determine the thermal contribution to the TAMs uplift. Seismic velocity variations in the upper mantle are dominantly caused by temperature changes, with S-waves being significantly more sensitive than P-waves (e.g., Priestley and McKenzie, 2013). We first calculated the absolute S-wave velocity variations associated with the RI and TNB anomalies as well as with the structure beneath EA. Then, following Faul and Jackson (2005), we related these velocity variations to associated temperature perturbations, which in turn can be used to estimate density changes (Lachenbruch and Morgan, 1990). The density differences between East Antarctica and the RI-TNB anomalies were then employed to determine the thermal load beneath the TAMs (see the Data Repository for further details).

Since total uplift estimates for the TAMs are varied (Fitzgerald, 2002, and references therein), we used the representative 1989 and 1997 models to assess if the imaged anomalous structure (Fig. 2) is consistent with a flexural origin. Both of these models estimate the uplift of the TAMs using ice, erosional, thermal, and end loads applied to a broken elastic plate. However, these studies assume different amounts of total uplift for the TAMs (5 km in the 1989 model; 7.2 km in the 1997 model) and employ different elastic plate thicknesses (Te; see the Data Repository). Using the thermal loading constraints based on our tomographic observations as well as erosional, ice, and end loads that are appropriate for the Transantarctic Mountains Seismic Experiment (TAMSEIS) and TAMNNET transects (Figs. DR12–DR15), we modeled the flexure along each seismic profile. The total uplift and Te values from both the 1989 and 1997 models were used to see if the corresponding flexure matched the observed bedrock topography (see the Data Repository).

As shown in Figure 3A, the overall shape of the TAMSEIS bedrock profile is well matched by both flexural models, with the 1997-equivalent model suggesting higher rates of exhumation. This indicates that the thermal load associated with the RI anomaly is consistent with flexural uplift along TAMSEIS. For the TAMNNET transect (Fig. 3B), the

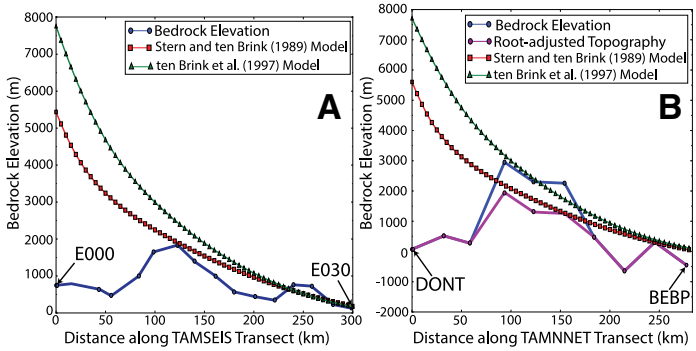

Figure 3. Bedrock topography from BEDMAP2 (blue lines; Fretwell et al., 2013) and modeled flexural profiles along the Transantarctic Mountains Seismic Experiment (TAMSEIS) (A) and the Transantarctic Mountains Northern Network (TAMNNET) (B) transects (Fig. 1). Red lines show 1989-equivalent model results, and green lines show 1997-equivalent model results. Purple line in B shows ~1 km adjusted bedrock topography. See text for details.

1997-equivalent model provides a better fit to the bedrock topography as compared to the 1989-equivalent model, since the elevations along TAMNNET are ~1 km higher than those on TAMSEIS. It is worth noting that Hansen et al. (2016) suggested that locally thicker crust may contribute to the higher TAMNNET elevations, though these crustal constraints are at the edge of their resolution. Assuming this ~1 km elevation difference can be attributed to local crustal effects, the adjusted bedrock topography is well fit by the 1989-equivalent model (Fig. 3B). In either case, the topography can be fit by the flexure profiles, indicating that the thermal load associated with the TNB anomaly is consistent with flexural uplift along TAMNNET. Additionally, flexural models similar to those described here also indicate that the lower-elevation Prince Albert Mountains (Fig. 1) may be associated with a long-wavelength flexural down-warp between RI and TNB (Fig. DR16).

Ultimately, our analysis demonstrates that thermal loading based on our tomographic models is consistent with a flexural origin for the TAMs. This thermal load plays a critical role in the uplift and elevations of the mountain range, where along-strike topographic variations can be explained by the variable upper-mantle structure imaged beneath the TAMs front.

ACKNOWLEDGMENTS

We thank the Incorporated Research Institutions for Seismology for providing PASSCAL data and field support. We also thank Dapeng Zhao for the inversion software, Tim Stern and Andrew Lloyd for method development, and Will Levandowski and two anonymous reviewers for their thorough critiques of this manuscript. Funding for this research was provided by National Science Foundation grant ANT-1148982.

REFERENCES CITED

Amante, C., and Eakins, B.C., 2009, ETOPO1 1 Arc-Minute Global Relief Model: Procedures, Data Sources, and Analysis: NOAA Technical Memorandum NESDIS NGDC-24: Boulder, Colorado, National Geophysical Data Center, NOAA, doi:10.7289/V5C8276M (accessed August 2015).

Bannister, S., Yu, J., Leitner, B., and Kennett, B.L.N., 2003, Variations in crustal structure across the transition from West to East Antarctica, southern Victoria Land: Geophysical Journal International, v. 155, p. 870–880, doi:10.1111/j.1365-246X.2003.02094.x.

Faul, U.H., and Jackson, I., 2005, The seismological signature of temperature and grain size variations in the upper mantle: Earth and Planetary Science Letters, v. 234, p. 119–134, doi:10.1016/j.epsl.2005.02.008.

Fitzgerald, P.G., 2002, Tectonics and landscape evolution of the Antarctic plate since the breakup of Gondwana, with an emphasis on the West Antarctic Rift System and the Transantarctic Mountains: Royal Society of New Zealand Bulletin, v. 35, p. 453–469.

Fretwell, P., et al., 2013, Bedmap2: Improved ice bed, surface and thickness datasets for Antarctica: The Cryosphere, v. 7, p. 375–393, doi:10.5194/tc-7-375-2013.

Graw, J.H., Adams, A.N., Hansen, S.E., Wiens, D.A., Hackworth, L., and Park, Y., 2016, Upper mantle shear wave velocity structure beneath northern Victoria Land, Antarctica: Volcanism and uplift in the northern Transantarctic Mountains: Earth and Planetary Science Letters, v. 449, p. 48–60, doi:10.1016/j.epsl.2016.05.026.

Hansen, S.E., Julia, J., Nyblade, A.A., Pyle, M.L., Wiens, D.A., and Anandakrishnan, S., 2009, Using S wave receiver functions to estimate crustal structure beneath ice sheets: An application to the Transantarctic Mountains and East Antarctic craton: Geochemistry Geophysics Geosystems, v. 10, Q08014, doi:10.1029/2009GC002576.

Hansen, S.E., Graw, J.H., Kenyon, L.M., Nyblade, A.A., Wiens, D.A., Aster, R.C., Huerta, A.D., Anandakrishnan, S., and Wilson, T., 2014, Imaging the Antarctic mantle using adaptively parameterized P-wave tomography: Evidence for heterogeneous structure beneath West Antarctica: Earth and Planetary Science Letters, v. 408, p. 66–78, doi:10.1016/j.epsl.2014.09.043.

Hansen, S.E., Reusch, A.M., Parker, T., Bloomquist, D.K., Carpenter, P., Graw, J.H., and Brenn, G.R., 2015, The Transantarctic Mountains Northern Network (TAMNNET): Deployment and performance of a seismic array in Antarctica: Seismological Research Letters, v. 86, p. 1636–1644, doi:10.1785/0220150117.

Hansen, S.E., Kenyon, L.M., Graw, J.H., Park, Y., and Nyblade, A.A., 2016, Crustal structure beneath the Northern Transantarctic Mountains and Wilkes Subglacial Basin: Implications for tectonic origins: Journal of Geophysical Research, v. 121, p. 812–825, doi:10.1002/2015JB012325.

Kennett, B.L.N., and Engdahl, E.R., 1991, Traveltimes for global earthquake location and phase identification: Geophysical Journal International, v. 105, p. 429–465, doi:10.1111/j.1365-246X.1991.tb06724.x.

Kyle, P.R., Moore, J.A., and Thrilwall, M.F., 1992, Petrologic evolution of anorthoclase phonolite lavas at Mt. Erebus, Ross Island, Antarctica: Journal of Petrology, v. 33, p. 849–875, doi:10.1093/petrology/33.4.849.

Lachenbruch, A.H., and Morgan, P., 1990, Continental extension, magmatism and elevation; formal relations and rules of thumb: Tectonophysics, v. 174, p. 39–62, doi:10.1016/0040-1951(90)90383-J.

Lawrence, J.F., Wiens, D.A., Nyblade, A.A., Anandakrishnan, S., Shore, P.J., and Voigt, D., 2006, Crust and upper mantle structure of the Transantarctic Mountains and surrounding regions from receiver functions, surface waves, and gravity: Implications for uplift models: Geochemistry Geophysics Geosystems, v. 7, Q10011, doi:10.1029/2006GC001282.

Lou, X., van der Lee, S., and Lloyd, S., 2013, AIMBAT: A Python/Matplotlib tool for measuring teleseismic arrival times: Seismological Research Letters, v. 84, p. 85–93, doi:10.1785/0220120033.

Morelli, A., and Danesi, S., 2004, Seismological imaging of the Antarctic continental lithosphere: A review: Global and Planetary Change, v. 42, p. 155–165, doi:10.1016/j.gloplacha.2003.12.005.

Park, Y., Yoo, H.J., Lee, W.S., Lee, C., Lee, J., Lee, H., Park, J., Kim, J., and Kim, Y., 2015, P-wave velocity structure beneath Mt. Melbourne in northern Victoria Land, Antarctica: Evidence of partial melting and volcanic magma sources: Earth and Planetary Science Letters, v. 432, p. 293–299, doi:10.1016/j.epsl.2015.10.015.

Priestley, K., and McKenzie, D., 2013, The relationship between shear wave velocity, temperature attenuation and viscosity in the shallow part of the mantle: Earth and Planetary Science Letters, v. 381, p. 78–91, doi:10.1016/j.epsl.2013.08.022.

Ramirez, C., Nyblade, A., Hansen, S.E., Wiens, D.A., Anandakrishnan, S., Aster, R.C., Huerta, A.D., Shore, P., and Wilson, T., 2016, Crustal and upper-mantle structure beneath ice-covered regions in Antarctica from S-wave receiver functions and implications for heat flow: Geophysical Journal International, v. 204, p. 1636–1648, doi:10.1093/gji/ggv542.

Reusch, A.M., Nyblade, A.A., Benoit, M.H., Wiens, D.A., Anandakrishnan, S., Voigt, D., and Shore, P.J., 2008, Mantle transition zone thickness beneath Ross Island, the Transantarctic Mountains and East Antarctica: Geophysical Research Letters, v. 35, L12301, doi:10.1029/2008GL033873.

Rocchi, S., Armienti, P., and Di Vincenzo, G., 2005, No plume, no rift magmatism in the West Antarctica Rift, *in* Foulger, G.R., et al., eds., Plates, Plumes, and Paradigms: Geological Society of America Special Paper 388, p. 435–447, doi:10.1130/2005.2388(26).

Sieminski, A., Debayle, E., and Leveque, J., 2003, Seismic evidence for deep low-velocity anomalies in the transition zone beneath West Antarctica: Earth and Planetary Science Letters, v. 216, p. 645–661, doi:10.1016/S0012-821X(03)00518-1.

Stern, T., and ten Brink, U.S., 1989, Flexural uplift of the Transantarctic Mountains: Journal of Geophysical Research, v. 94, p. 10315–10330, doi:10.1029/JB094iB08p10315.

Studinger, M., Bell, R.E., Buck, W.R., Karner, G.D., and Blankenship, D.D., 2004, Sub-ice geology inland of the Transantarctic Mountains in light of new aerogeophysical data: Earth and Planetary Science Letters, v. 220, p. 391–408, doi:10.1016/S0012-821X(04)00066-4.

ten Brink, U.S., Hackney, R.I., Bannister, S., Stern, T.A., and Makovsky, Y., 1997, Uplift of the Transantarctic Mountains and the bedrock beneath the East Antarctic Ice Sheet: Journal of Geophysical Research, v. 102, p. 27603–27621, doi:10.1029/97JB02483.

VanDecar, J.C., and Crosson, R.S., 1990, Determination of teleseismic relative phase arrival times using multi-channel cross-correlation and least squares: Bulletin of the Seismological Society of America, v. 80, p. 150–169.

Wang, Y., Forsyth, D.W., and Savage, B., 2009, Convective upwelling in the mantle beneath the Gulf of California: Nature, v. 462, p. 499–501, doi:10.1038/nature08552.

Watson, T., Nyblade, A.A., Wiens, D.A., Anandakrishnan, S., Benoit, M., Shore, P.J., Voigt, D., and VanDecar, J.C., 2006, P and S velocity structure of the upper mantle beneath the Transantarctic Mountains, East Antarctic craton, and Ross Sea from travel time tomography: Geochemistry Geophysics Geosystems, v. 7, Q07005, doi:10.1029/2005GC001238.

Zhao, D., Hasegawa, A., and Kanamori, H., 1994, Deep structure of Japan subduction zone as derived from local, regional, and teleseismic events: Journal of Geophysical Research, v. 99, p. 22313–22329, doi:10.1029/94JB01149.

Manuscript received 9 November 2016
Revised manuscript received 23 January 2017
Manuscript accepted 27 January 2017

Printed in USA